Feasibility study of measuring interaction cross sections of hypernuclei produced in projectile fragmentation reactions with WASA-FRS setup

Yiming Gao (高亦鸣)^{1,2,3†} Yoshiki K. Tanaka² Vasyl Drozd^{4,5} Hiroyuki Ekawa² Samuel Escrig⁶ Yan He (何燕)^{2,7} Ayumi Kasagi^{2,8,9} Enqiang Liu (刘恩强)^{1,2,3} Manami Nakagawa² Christophe Rappold⁶ Takehiko R. Saito^{2,5,7} Ryohei Sekiya^{10,11} He Wang (王赫)^{1,2} Ayari Yanai^{2,12} Xiaohong Zhou (周小红)¹

¹Institute of Modern Physics, Chinese Academy of Sciences, Lanzhou 730000, China
²High Energy Nuclear Physics Laboratory, RIKEN, 351-0198 Wako, Saitama, Japan
³School of Nuclear Science and Technology, University of Chinese Academy of Sciences, Beijing 100049, China
⁴University of Groningen, 9747 AA Groningen, The Netherlands
⁵GSI Helmholtzzentrum für Schwerionenforschung GmbH, 64291 Darmstadt, Germany
⁶Instituto de Estructura de la Materia - CSIC, 28006 Madrid, Spain
⁷School of Nuclear Science and Technology, Lanzhou University, Lanzhou 730000, China
⁸Graduate School of Engineering, Gifu University, 501-1193 Gifu, Japan
⁹Graduate School of Artificial Intelligence and Science, Rikkyo University, 171-8501 Tokyo, Japan
¹⁰Department of Physics, Kyoto University, 606-8502 Kyoto, Japan
¹¹RIKEN Nishina Center for Accelerator-Based Science, RIKEN, 351-0198 Wako, Saitama, Japan
¹²Saitama University, 338-8570 Sakura-ku, Saitama, Japan

Abstract: A novel method is proposed to measure the interaction cross sections of short-lived hypernuclei with the WASA-FRS experimental setup at GSI and FAIR. The interaction cross sections of hypernuclei, produced in projectile fragmentation reactions at relativistic energies, can be determined from their production point distribution within a target. The feasibility of such a measurement is evaluated through detailed Monte Carlo simulations. The results indicate that an aimed uncertainty on the order of 10% can be achieved for the case of a hypertriton, demonstrating the potential of this method for studying matter radii and the possible hyperon halo structure of hypernuclei.

Keywords: hypernuclear interaction cross section, hypertriton, Λ halo, projectile fragmentation reaction, fragment separator, Monte Carlo simulation, scintillating fiber detector

DOI: 10.1088/1674-1137/adf4b2 **CSTR:** 32044.14.ChinesePhysicsC.49124003

I. INTRODUCTION

The interactions among baryons under the flavor SU(3) symmetry, which includes up, down, and strange quarks, represent a fundamental aspect of strong interactions. While interactions between ordinary nucleons have been experimentally studied in detail, the knowledge of those involving at least one or more hyperons remains limited [1]. Only small amounts of experimental data are available for hyperon-nucleon scattering, and no data are available for hyperon-hyperon scattering, as the relatively short lifetimes of hyperons, typically on the order of 10^{-10} s, make such direct experiments challenging. In this context, experimental investigations of hypernuclei, particularly single and double Λ -hypernuclei, have played an important role in exploring hyperon-nucleon and hyperon-hyperon interactions.

The hypertriton (${}_{\Lambda}^{3}$ H), consisting of a proton, neutron, and Λ hyperon, is the lightest known hypernucleus,

serving as a benchmark in the field of hypernuclear physics [2]. Extensive efforts have been undertaken to determine its properties, such as the Λ binding energy and lifetime, with different experimental approaches [3–7]. Earlier experimental studies using nuclear emulsion techniques in the 1970s obtained the Λ binding energy to the deuteron core of 0.13 ± 0.05 MeV [8], which has served as a crucial input for the theoretical calculations of hypernuclei [9, 10]. Recent studies on ultra-relativistic heavyion collision experiments have evaluated the binding energy to be 0.41±0.12(stat.)±0.11(syst.) MeV [11] and 0.102±0.063(stat.)±0.067(syst.) MeV [12] using the STAR and ALICE collaborations, respectively. Further efforts to achieve unprecedented precision on the binding energy are underway, including the J-PARC E07 experiment employing machine-learning techniques [13, 14] and the decay-pion spectroscopy experiment at the MAMI facility [15].

One of the intriguing features of a hypertriton is its

Received 30 June 2025; Accepted 25 July 2025; Published online 26 July 2025

[†] E-mail: gaoym@impcas.ac.cn

^{©2025} Chinese Physical Society and the Institute of High Energy Physics of the Chinese Academy of Sciences and the Institute of Modern Physics of the Chinese Academy of Sciences and IOP Publishing Ltd. All rights, including for text and data mining, AI training, and similar technologies, are reserved.

expected Λ -halo structure, arising from the weak binding of the Λ hyperon to the deuteron core. A large root-mean-square matter radius of ~ 5 fm has been predicted for a Λ binding energy of 0.13 MeV, whereas theoretical studies have shown a strong dependence of the radius on the binding energy [16, 17]. So far, there has been no direct measurement of the matter radius of $^3_\Lambda H$, owing to experimental challenges originating from its low production rate and short lifetime. Nevertheless, if realized, such measurements would offer valuable insights into the structures and underlying interactions of hypernuclei.

The nuclear matter distribution of short-lived unstable nuclei has been extensively studied, leading to the unveiling of exotic structures, such as nuclear halos and skins [18-20], since the pioneering discovery of the twoneutron halo in ¹¹Li [21, 22]. The interaction cross section, defined as the sum of the cross sections for all reactions that change the identity of the projectile (i.e., the number of protons or neutrons), provides a measure to deduce the root-mean-square matter radius through the Glauber model reaction theory. The transmission method [23] is employed to experimentally determine the interaction cross section, where the ratio of the number of incident projectiles on a target to the number of outgoing unreacted projectiles is measured. This technique requires inflight separated and identified beams of the nuclei of interest, which can be performed using fragment separator facilities [24, 25]. For instance, the interaction cross sections of ³¹Ne [26] and ²⁹F [27] were measured with the BigRIPS [28] at RIBF, and that of ²³O [29] was measured with the Fragment Separator (FRS) [30] at GSI. However, this method is practically challenging in the case of hypernuclei owing to their very short lifetimes, typically on the order of a few hundred picoseconds. Therefore, alternative approaches are required to probe hypernuclear interaction cross sections.

To realize the experimental studies of the $^3_\Lambda H$ halo structure, we propose a novel method for measuring the interaction cross sections of hypernuclei produced via projectile fragmentation reactions with relativistic heavyion beams. The core concept of the method is to utilize the reconstructed production point distribution of $^3_\Lambda H$ within a production target, taking advantage of in-flight hypernuclei and the Wide Angle Shower Apparatus (WASA)-FRS experimental setup at GSI and FAIR [31]. This approach is complementary to the forthcoming experiment proposed by the R3B collaboration at GSI and FAIR with the HYDRA experimental setup [32], which focuses on measuring decay-vertex distributions in two independent measurements with different target thickness setups.

In this study, we investigate the feasibility of the proposed experiment for measuring hypernuclear interaction cross sections using Monte Carlo simulations. In Sec. II, we describe the principle of the proposed method. In Sec.

III, we introduce the experimental method utilizing the WASA-FRS hypernuclear experimental setup at GSI and FAIR. In Sec. IV, we discuss the feasibility of extracting the interaction cross section and possible improvements to the experimental setup for future experiments. Finally, a summary is provided in Sec. V.

II. EXPERIMENTAL PRINCIPLE

In the present investigation, we aim to determine the interaction cross section of ${}^3_\Lambda H$ with a carbon target, hereafter referred to as $\sigma_{I({}^3_\Lambda H)}$, with a relative uncertainty of the order of 10%. The proposed method involves deducing $\sigma_{I({}^3_\Lambda H)}$ from the reconstructed production point distribution of ${}^3_\Lambda H$ in the target. The interaction cross section can be extracted from a slope of the production point distribution, as the slope reflects the attenuation of ${}^3_\Lambda H$ along the target material owing to its interaction with target nuclei. The detailed principle is formulated in this section.

In the WASA-FRS hypernuclear experiment, relativistic 6 Li ions at 2 GeV/u impinge on a fixed carbon target to produce in-flight $^3_\Lambda$ H. The $^3_\Lambda$ H hypernuclei are produced via projectile fragmentation followed by capturing a Λ hyperon created in a hot participant region of the collision. As the forward emitted $^3_\Lambda$ H has a velocity similar to that of the primary beam, the decay length of $^3_\Lambda$ H in the laboratory frame is on the order of 20 cm owing to the Lorentz boost. The invariant-mass spectroscopy method is employed to identify the events associated with $^3_\Lambda$ H, by measuring the momenta of all the decay products, particularly π^- and 3 He, via the mesonic two-body decay mode.

The production point of ${}^3_{\Lambda} H$ within the target material can be reconstructed by measuring light charged particles (e.g., π^{\pm} , K^{+} , and proton) produced in the primary reaction. As the particles created in the participant zone of the collision have a broad angular distribution, in contrast to that measured for the forward ${}^3_{\Lambda} H$, their trajectories in combination with the incident beam track constrain the production point of ${}^3_{\Lambda} H$ with a reasonable resolution. A simulation with the ultra-relativistic quantum molecular dynamics (UrQMD) model [33, 34] predicts the average number of emitted particles to be 4.7, in coincidence with the forward ${}^3_{\Lambda} H$. This multiplicity enables the efficient reconstruction of the production point, as demonstrated in a detailed simulation in Sec. IV.

The reconstructed production point distribution $PPD_{reco}(z)$ for the ${}^3_{\Lambda}H$ -identified events is proportional to the following two factors in terms of its z dependence within the target material: (i) the real production point distribution $PPD_{all}(z)$ and (ii) survival probability $P_{surv}(z)$ of ${}^3_{\Lambda}H$ from the production point z to the exit surface of the target. Here, we adopt the z axis along the direction of the primary beam with z=0 and $z=z_T$ being at the entrance and exit planes of the target, respectively. Other

factors, such as the branching ratio of the ${}^{3}_{\Lambda}H \rightarrow \pi^{-} + {}^{3}He$ decay mode or the survival probability of ${}^{3}_{\Lambda}H$ after the exit of the target, are common for different production points z and thus do not affect the following discussions based on the z dependence.

The first factor $PPD_{all}(z)$ includes all events associated with the hypertriton production and is expressed by

$$PPD_{all}(z) = dN_{\Lambda}^{3} H/dz$$

$$= n \cdot \sigma_{P(_{\Lambda}^{3} H)} \cdot N_{0} \cdot e^{-n\sigma_{I(_{\Gamma}^{6} Li)} z}, \qquad (1)$$

where dN_{3H} represents the number of ${}_{\Lambda}^{3}H$ produced in a region [z, z+dz]. The symbol *n* denotes the target particle density, and N_0 denotes the initial number of primary ⁶Li beam particles at the entrance of the target (z = 0). $\sigma_{P_{\lambda}^{3}H}$ is the production cross section of the ${}_{\Lambda}^{3}H$ in the ${}^{6}Li+{}^{12}C$ reaction, which was evaluated to be $3.9 \pm 1.4 \mu b$ in the former HypHI experiment at GSI [35]. $\sigma_{I^{(6}Li)}$ represents the interaction cross section of ⁶Li with a carbon target, which was measured to be 688±10 mb at 790 MeV/u [21]. Here, we assume the same value in the present investigation, as the averaged nucleon-nucleon total cross section is approximately the same for high energies [36]. However, a measurement of $\sigma_{I(^6\text{Li})}$ directly at the energy of interest would be important for future precise investigations to avoid the uncertainties arising from the energy dependence of the nuclear-nuclear interaction cross sections.

The second factor, survival probability $P_{\text{surv}}(z)$, is given by

$$P_{\text{surv}}(z) = e^{-\left(n\sigma_{I(_{\Lambda}^{3}\text{H})} + \frac{1}{\gamma\beta c\tau}\right)(z_{\text{T}} - z)},$$
(2)

where the parameters β and γ are the velocity of the ${}^3_{\Lambda}H$ relative to the speed of light c and the Lorentz factor, respectively. τ represents the ${}^3_{\Lambda}H$ lifetime, which has the averaged value of 237 ± 10 ps [12, 37, 38].

From Eqs. (1) and (2), the z-dependence of the reconstructed production point distribution $PPD_{reco}(z)$ is given as

$$\begin{split} \text{PPD}_{\text{reco}}(z) &\propto \text{PPD}_{\text{all}}(z) \cdot P_{\text{surv}}(z) \\ &\propto e^{\left(n\sigma_{I_{\Lambda}^{(3)}\text{H}}\right)^{\frac{1}{\gamma\beta\text{cr}}} - n\sigma_{I_{\Lambda}^{(6}\text{Li})}\right)^{z}}. \end{split} \tag{3}$$

Figure 1 (a), (b), and (c) show PPD_{all}(z), $P_{\text{surv}}(z)$, and PPD_{reco}(z) for three different cases of $\sigma_{I_{\alpha}^{3}\text{H})}$ at 0, 0.65, and 0.85 b, respectively. Note that $\sigma_{I_{\alpha}^{3}\text{H})} = 0.65$ and 0.85 b approximately correspond to the predicted values for the Λ -binding energies of 0.41 and 0.13 keV, respectively, as calculated in Ref. [32]. Here, we assumed a diamond tar-

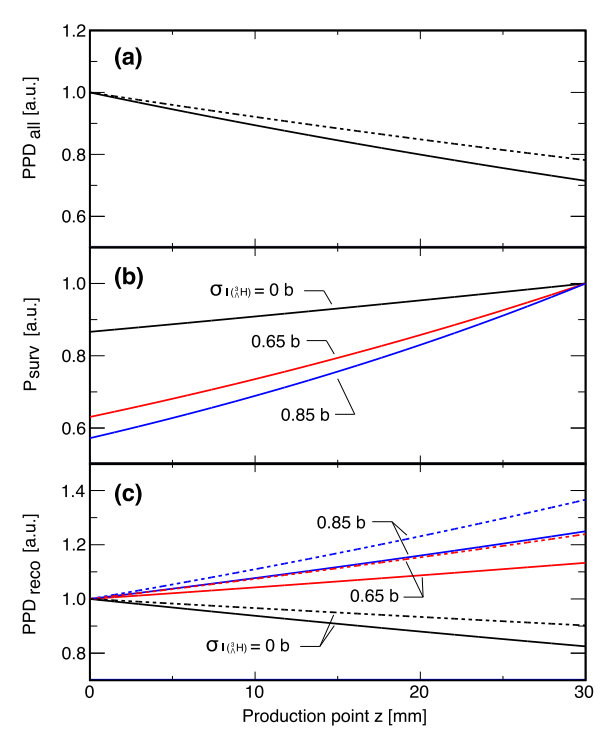


Fig. 1. (color online) (a) Illustration of production point distribution PPD_{all}(z) along the beam direction z. (b) Survival probability $P_{\text{surv}}(z)$ of $_{\Lambda}^{3}$ H from the production point z to the exit of the target (z=3 cm). The colors correspond to differently assumed interaction cross sections of $\sigma_{I_{\Lambda}^{3}\text{H})}=0$ b (black), 0.65 b (red), and 0.85 b (blue). (c) Reconstructed production point distribution PPD_{reco}(z). The solid curves represent the results obtained only with the direct $_{\Lambda}^{3}$ H production, and the dashed curves include a contribution of the two-step process with intermediate $_{\Lambda}^{4}$ He.

get $(n=1.6\times10^{23}~{\rm cm^{-3}})$ with a thickness of $z_{\rm T}=3~{\rm cm}$ based on the experimental setup of the first WASA-FRS experiment in 2022. The difference of 0.2 b, from $\sigma_{I(^3_{\Lambda}{\rm H})}=0.85~{\rm b}$ to 0.65 b, leads to a detectable difference in the exponential slope of approximately 43%. The uncertainties associated with $\sigma_{I(^6{\rm Li})}$ and τ result in errors of 10 mb and 12 mb, respectively. Therefore, the aimed uncertainty of $\sigma_{I(^3_{\Lambda}{\rm H})}$ on the order of 10% can, in principle, be achieved with this method, provided that a sufficient amount of statistics is accumulated and other experimental systematic errors are well controlled. The details of these conditions are discussed in Sec. IV.

Furthermore, we evaluate the influence of the twostep strangeness production, which refers to the production of ${}^3_\Lambda H$ via other secondary fragments. Such processes introduce an additional term of the form

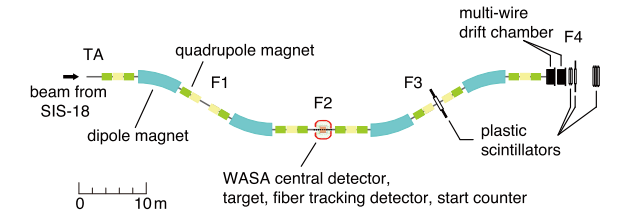
$$PPD_{\text{all}}^{(2)}(z) = \sum_{X} N_0 n \sigma_{P(X \to {}_{\Lambda}^3 \text{H})} \frac{\sigma_{P(X)}}{\sigma_{I(X)} - \sigma_{I({}^6 \text{Li})}}$$

$$(e^{-\sigma_{I({}^6 \text{Li})} n z} - e^{-\sigma_{I(X)} n z})$$
(4)

to be added in PPD_{all}(z) in Eq. (1), where $\sigma_{P(X)}$, $\sigma_{I(X)}$, and $\sigma_{P(X\to^3 H)}$ represent the production cross section of an intermediate fragment X from the primary beam, the interaction cross section of X, and the $^3_{\Lambda}$ H production cross section from X, respectively. The dashed curves in Panels (a) and (c) illustrate the effects owing to the secondary ³_AH production via intermediate ⁴He, which we estimate to have the dominant contribution. Here, we assumed $\sigma_I(^4\text{He}) = 503 \text{ mb from Ref. } [39], \ \sigma_P(^4\text{He}) = 239 \text{ mb es}$ timated by the Liége intranuclear cascade model (INCL++) [40, 41], and $\sigma_{P(X \to {}^{3}\text{H})} = 3.0 \text{ }\mu\text{b}$ obtained with the Dubna cascade model (DCM-QGSM) [42]. Although the total amount of the reconstructed ³_AH owing to this two-step process is only 4%, it predominantly contributes to larger z in PPD_{reco}(z) and affects the overall slope of the distribution, as displayed in Panel (c) of Fig. 1. This leads to a bias in the determination of $\sigma_{I(^3H)}$ as large as 28%, if the two-step process contribution is ignored in the extraction of $\sigma_{I(^3H)}$. Thus, this contribution cannot be overlooked. Its evaluation and correction will become important for future precise measurements.

III. EXPERIMENTAL SETUP

The experiment utilizes the WASA-FRS setup integrating the central part of the WASA [43] into the FRS at GSI [30]. The general layout is shown in the top panel of Fig. 2. A ⁶Li beam at a relativistic energy of 2 GeV/u accelerated by the synchrotron SIS-18 is transported to the F2 focal plane of the FRS, where a ¹²C target and the WASA detector system are installed. Light hypernuclei are produced in a projectile fragmentation reaction with the target, and particles emitted from mesonic two-body decay (e.g., π^- and ³He from hypertriton) are measured to obtain the invariant-mass and decay vertex distributions. The F2-F4 section of the FRS is operated as a high-resolution spectrometer to analyze the momentum of the forward residue (e.g., 3 He), whereas the π^{-} is measured with the WASA and additional detectors in F2 with a large solid angle. The lower panel of Fig. 2 shows a detailed configuration at F2 [44] and a typical event topology. The target is placed at the entrance of the WASA detector, which consists of a superconducting solenoid magnet [45], a mini drift chamber (MDC) [46], a plastic scintillator barrel (PSB) and its end-caps (PSFE, PSBE) [47], and an electromagnetic calorimeter [48]. In addition, a compact start timing counter [49] and sets of tracking detectors based on scintillating fibers with a diameter of 0.5 mm (UFT1-3, MFT1-2, DFT1-2) are installed for the hypernuclear experiment. The upstream detectors UFT1 and UFT2 measure the trajectory of the primary 6Li beam, and the downstream ones DFT1 and DFT2 are used for the forward heavy residue. The track of the decay π^- is reconstructed by UFT3, MFT1, and MFT2 in combination with MDC. Furthermore, other charged



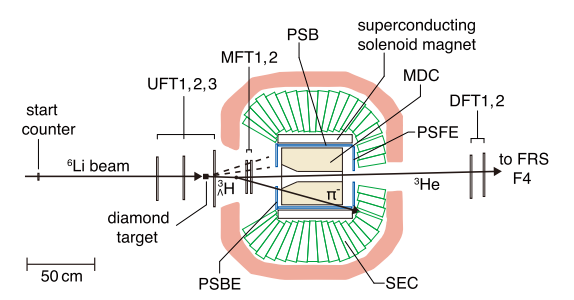


Fig. 2. (color online) (Top panel) Schematic of the WASA-FRS experimental setup. The WASA central detectors are integrated into the FRS. A beam from the synchrotron SIS-18 impinges on a target at F2. The F2–F4 section of the FRS is used to analyze emitted particles at forward 0° , which are measured with plastic scintillators at F3 and F4 and with multi-wire drift chambers at F4. (Bottom panel) Detailed view of the experimental setup at F2 for the WASA-FRS hypernuclear experiment. A diamond target, a start timing counter, and scintillating-fiber tracking detectors are installed in addition to the WASA central detector system. A typical event topology of a hypertriton decay into π^- and 3 He is also shown. The dashed lines indicate light charged particles emitted from the primary reaction. See the text for details.

particles emitted in the primary reaction are recorded by UFT3, MFT1, and MFT2, which provide information on the production vertex position essential for the present investigation. The high-granularity of these fiber trackers fulfills the requirement for reconstructing the production point under high particle rate and multiplicity conditions.

The first pilot run of the WASA-FRS hypernuclear experiment was performed in 2022 with the goal of the precise determination of the lifetime of ${}_{\Lambda}^{3}H$ and ${}_{\Lambda}^{4}H$ and of neutral ${}_{\Lambda}^{3}n$ signals to solve the puzzles raised by the former experiments [38, 50, 51]. Data for the hypertriton channel were accumulated for approximately 41 h with the FRS magnetic rigidity set for ${}^{3}He$. The analysis of the experiment data is currently in progress [44, 52, 53].

IV. FEASIBILITY INVESTIGATION

A. Original WASA-FRS-HypHI setup

To investigate the feasibility of measuring the production point distribution with the WASA-FRS HypHI experimental setup, we performed Monte Carlo simulations using a Geant4 toolkit [54–56]. Events were generated at

different z positions in the target following the distribution defined by Eq. (1), where a hypertriton and light charged particles were produced based on a simulation of the $^6\text{Li}+^{12}\text{C}$ reaction at 2 A GeV with the UrQMD model and kinematical cuts described in Ref. [57]. The hypertriton was propagated in the target assuming the survival probability given in Eq. (2) with $\sigma_I = 0.85$ b, and then, its mesonic two-body decay $^{\text{A}}_{\text{A}}\text{H} \rightarrow \pi^- + ^3\text{He}$ was simulated.

The hypertriton was identified by invariant-mass spectroscopy at the first step of the analysis. The momentum of the π^- was obtained with a resolution in the range of 6%-10% by fitting trajectories recorded in MFT1, MFT2, MDC, and PSB or PSFE with a Kalman filter algorithm [58] or by employing a machine learning technique with a graph neural network [59]. The ³He momentum was analyzed by the forward spectrometer FRS with a high resolution of approximately 1×10^{-4} , operated at a magnetic rigidity of 12.5 Tm. These steps led to the invariant-mass resolution of 3.2 MeV/ c^2 [2, 59], which allowed us to identify the hypertriton events for subsequent analysis. The abovementioned UrQMD simulation predicted a kinetic-energy of 5.93 ± 0.29 GeV within one standard deviation for the produced projectile-like hypertritons and 5.67 ± 0.16 GeV for the hypertritons identified via the coincident detection of π^- and ³He by the WASA and FRS, respectively, based on Geant4 and ion-optical transport [60] simulations. Furthermore, we selected events with a decay vertex position more than 4 cm behind the target, as in the experimental analysis.

Next, the production point of ${}_{\Lambda}^{3}H$ was analyzed by using the trajectories of the primary ${}^{6}Li$ and the produced light charged particles in the reaction except for ${}_{\Lambda}^{3}H$ and its decay particles. The ${}^{6}Li$ track was reconstructed from hits recorded in the upstream tracking detectors UFT1 and UFT2, whereas the tracks of the light particles were obtained by UFT-3, MFT-1, and MFT-2. We eliminated the light particles with the number of hit fiber layers less than 5 to enhance the z resolution of the production point. A topological vertex reconstruction algorithm [61] was employed to determine the production vertex from the adopted trajectories and their covariance matrices.

The resolution and efficiency of the production point reconstruction were evaluated to characterize the analysis performance. We observed the residual distribution of the production point z, which is defined by the difference between a true production point z and a reconstructed one and has a shape with a long tail structure that can be fitted by a Cauchy function. The top panel in Fig. 3 shows the obtained z resolution defined by its full width at half maximum as a function of the z coordinate. The resolution varies from 6 mm to 4 mm depending on the z position in the target. As displayed in the bottom panel, a z-dependent trend is also observed for the efficiency of the production point reconstruction, which is defined as the probability of reconstructing the production point, under

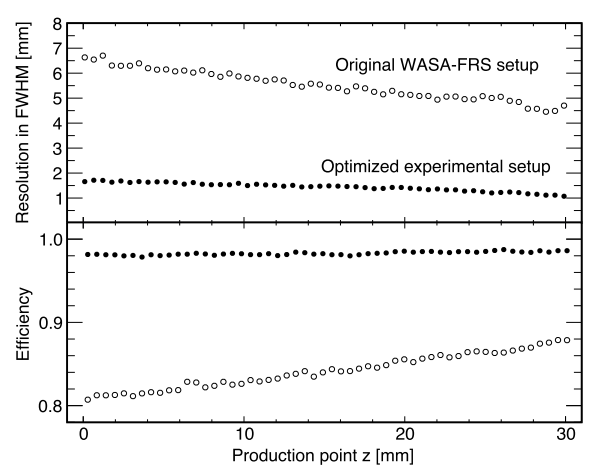


Fig. 3. (Top panel) Evaluated resolution for reconstructing the production point as a function of the production point z, based on Monte Carlo simulations. (Bottom panel) Evaluated efficiency of production point reconstruction as a function of the production point z. The open and closed circles represent the results obtained with the original WASA-FRS setup (Sec. IV.A) and the optimized setup (Sec. IV.B), respectively.

the condition that the hypertriton was identified through the detection of ${}^{3}\text{He}$ and π^{-} . Such z dependence is explained by the interactions of the produced light particles within the target and geometrical acceptance.

Reconstructed production point distribution with the simulated data is presented by the blue line in Fig. 4 for a total of 10^4 hypertriton-identified events. The distribution exhibits a similar slope to the true curve, shown by the black line, assumed in the simulation, but its detailed shape is modified owing to the z-dependent resolution

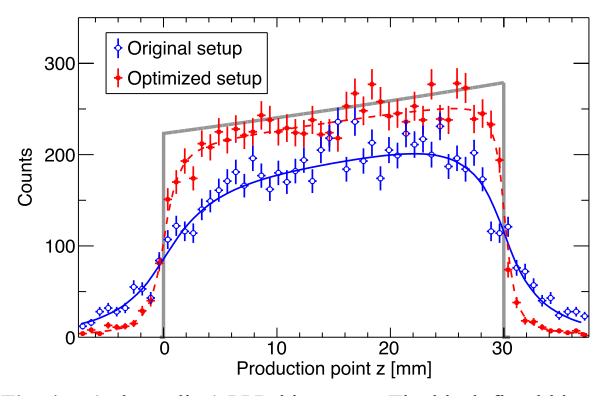


Fig. 4. (color online) PPD histogram: The black fitted histogram represents the input PPD of this simulation. The blue fitted histogram depicts the PPD measured with the original WASA-FRS HypHI setup, where beam product tracks are reconstructed by UFT3, MFT1, and MFT2, and the production point is identified using the vertex finding algorithm. The red fitted histogram represents the PPD measured with a pair of larger UFT3 (UFT3 and UFT4) using the same analysis procedure.

and efficiency. Therefore, the distribution needs to be fitted by the exponential function in Eq. (3) convoluted with the z-dependent resolution and scaled by the z-dependent efficiency curve, as shown in Fig. 3. The value of the interaction cross section thus fitted is $\sigma_{I_{\Lambda}^{3}H)} = 0.860 \pm 0.092$ b, which is consistent with the input value of 0.85 b in the simulation. This demonstrates that a statistical uncertainty of 10% can be achieved with $\sim 10^4$ hypertriton events, which is feasible in a realistic amount of beam time, assuming the same experimental condition as that considered in Ref. [2].

B. Optimized experimental setup

However, the above analysis with the existing WASA-FRS HypHI setup relies on the evaluation of the z-dependent resolution and efficiency based on the Monte Carlo simulations. In fact, neglecting the z-dependence in the fitting results in an overestimation of the interaction cross section by 38%. Thus, this would introduce an additional systematic uncertainty in a real experimental case. To address this issue, we discuss an improved setup optimized for the present purpose.

Here, we propose to implement two modifications: (i) use a reaction target with smaller transverse dimensions and (ii) install an additional large tracking detector behind UFT3. The former is to minimize the scattering of the forward emitted light particles within the target, whereas the latter extends the angular acceptance for measuring these particles. Thus, both modifications contribute to increasing the number of available particles reaching sufficient layers of the tracking detectors and available for production vertex analysis, as observed in Fig. 5. For an experimental setup, we considered a cylindrical target with a diameter of 10 mm and a scintillating fiber detector twice as large as UFT3, denoted by UFT4, for further evaluation.

The expected performance of the production point reconstruction with the modified setup is summarized in Table 1. We tested different values for the distance d between the middle points of UFT3 and UFT4 from 0 cm to 15 cm. We adopted the case with d = 5 cm and with a smaller target, which yielded the highest gains in terms of resolution and efficiency. The solid black points in Fig. 3 display the improved resolution and efficiency as a function of the z coordinate for the adopted case.

The reconstructed production point distribution obtained with the optimized setup is shown by the red histogram in Fig. 4. The distribution exhibits clear improvements in both resolution and efficiency; the edge of the distribution becomes sharper, and the number of events with reconstructed production points within the target region is increased by 21%. The red dashed curve shows the fit results, yielding $\sigma_{I_{\Lambda}^3H} = 0.818 \pm 0.076$ b. As the resolution and efficiency show less dependence on the *z*-position, the systematic uncertainty in the estimation of

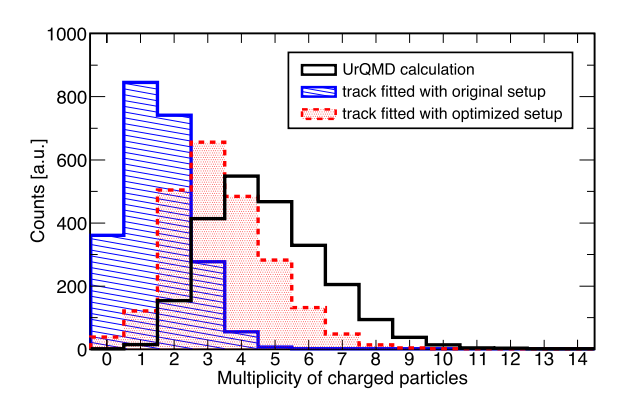


Fig. 5. (color online) Multiplicity of light charged particles (proton, π^{\pm} , K^{+}) emitted from the primary $^{6}\text{Li} + ^{12}\text{Cinteractions}$ in hypertriton production events. The hypertriton and its decay products are excluded from the multiplicity count. The black histogram includes all particles generated by the Ur-QMD calculation. The blue and red histograms represent the multiplicity of particles reaching sufficient layers of the fiber detectors for track fitting in the original WASA-FRS setup (Sec. IV.A) and optimized setup (Sec. IV.B), respectively.

Table 1. Evaluated resolution and efficiency for reconstructing the production point z for different experimental configurations. The mean values represent the averaged value in the z region of interest (0 mm $\le z \le 30$ mm), whereas the differences represent changes in the values from z = 0 mm to z = 30 mm

UFT4	Target -	Resolution/mm		Efficiency	
		mean	difference	mean	difference
no UFT4	original	5.51	-1.94	0.841	0.070
at $d = 0$ cm	original	2.49	-2.13	0.981	0.011
at $d = 5$ cm	original	1.67	-1.14	0.982	0.010
at $d = 10 \text{ cm}$	original	1.70	-1.17	0.980	0.012
at $d = 15$ cm	original	1.81	-1.20	0.979	0.014
at $d = 5$ cm	small	1.44	-0.59	0.983	0.006

the interaction cross section arising from their evaluation can be significantly reduced.

V. SUMMARY

The feasibility of a novel approach to measure the interaction cross section of ${}^{3}_{\Lambda}$ H, utilizing the WASA-FRS experimental setup at GSI and FAIR, was explored. In addition to the settings modified in this study, the development of a silicon micro-vertex detection system for obtaining good primary vertex measurement, as in Ref. [62], was considered. Investigations based on detailed Monte Carlo simulations demonstrated that the interaction cross section can be determined with an uncertainty on the order of 10% by reconstructing the production point distri-

bution within the production target. These results highlight the potential of this method for studying matter radii

and exploring possible hyperon halo structures in hypernuclei.

References

- [1] K. Miwa, K. Nakazawa, H. Tamura *et al.*, Eur. Phys. J. A **61**, 128 (2025)
- [2] T. R. Saito, W. Dou, V. Drozd *et al.*, Nat. Rev. Phys. **3**, 803 (2021)
- [3] D. H. Davis, Nucl. Phys. A **754**, 3 (2005)
- 4] D. H. Davis, Nucl. Phys. A **754**, 14 (2005)
- [5] O. Hashimoto and H. Tamura, Prog. Part. Nucl. Phys. **57**(2), 564 (2006)
- [6] A. Feliciello and T. Nagae, Rep. Prog. Phys. 78, 096301 (2015)
- [7] J. Chen, L. Geng, E. Hitama *et al.*, arXiv: 2506.00864
- [8] M. Jurič, G. Bohm, J. Klabuhn *et al.*, Nucl. Phys. B **52**, 1 (1973)
- [9] D. Lonardoni, A. Lovato, S. Gandolfi *et al.*, Phys. Rev. Lett. 114, 092301 (2015)
- [10] L. Contessi and N. Barnea, A. Gal, Phys. Rev. Lett. 121, 102502 (2018)
- [11] STAR Collaboration, Nat. Phys. 16(4), 409 (2020)
- [12] S. Acharya *et al.* (ALICE Collaboration), Phys. Rev. Lett. **131**, 102302 (2023)
- [13] A. Kasagi, W. Dou, V. Drozd *et al.*, Nucl. Instrum. Methods Phys. Res. A **1056**, 168663 (2023)
- [14] A. Kasagi, T. R. Saito, V. Drozd et al., arXiv: 2504.01601
- [15] P. Eckert, P. Achenbach, T. Akiyama *et al.*, EPJ Web of Conferences **271**, 01006 (2022)
- [16] H. Nemura, Y. Suzuki, Y. Fujiwara et al., Prog. Theor. Phys. 103, 929 (2000)
- [17] F.Hildenbrand and H. W. Hammer, Phys. Rev. C **100**, 034002 (2019)
- [18] I. Tanihata, J. Phys. G: Nucl. Part. Phys. 22, 157 (1996)
- [19] A. Ozawa, T. Suzuki, and I. Tanihata, Nucl. Phys. A 693, 32 (2001)
- [20] I. Tanihata, H. Savajols, and R. Kanungo, Prog. Part. Nucl. Phys. A 68, 215 (2013)
- [21] I. Tanihata, H. Hamagaki, O. Hashimoto *et al.*, Phys. Rev. Lett. **55**, 2676 (1985)
- [22] P. G. Hansen and B. Jonson, Europhys. Lett. 4, 409 (1987)
- [23] G. Giacomelli, in *Total Cross-Section Measurements*, Chap. 2, edited by D. M. Brink and J. H. Mulvey (Pergamon, 1970), p.81
- [24] H. Geissel and D. J. Morrissey, in *Handbook of Nuclear Physics*, *Exotic Nuclei and Their Separation*, *Electromagnetic Devices*, edited by I. Tanihata, H. Toki, and T. Kajino (Springer Nature Singapore, 2020), p.1
- [25] H. Geissel and D. J. Morrissey, in *Handbook of Nuclear Physics, Exotic Nuclei and Their Separation, Using Atomic Interactions*, edited by I. Tanihata, H. Toki, and T. Kajino (Singapore: Springer Nature, 2020), p.63
- [26] M. Takechi, T. Ohtsubo, M. Fukuda et al., Phys. Lett. B 707, 357 (2012)
- [27] S. Bagchi, R. Kanungo, Y. K. Tanaka et al., Phys. Rev. Lett. 124, 222504 (2020)
- [28] T. Kubo, Nucl. Instrum. Methods Phys. Res., Sect. B **204**, 97 (2003)
- [29] A. Ozawa, O. Bochkarev, L. Chulkov et al., Nucl. Phys. A 691, 599 (2001)
- [30] H. Geissel, P. Armbruster, K. H. Bchr et al., Nucl. Instrum. Methods Phys. Res. B 70, 286 (1992)
- [31] T. R. Saito, S. Bagchi, K. H. Behr et al., Studies of the $d+\pi^-$ signal and lifetime of the ${}_{\Lambda}^3H$ and ${}_{\Lambda}^4H$ hypernuclei by new spectroscopy techniques with FRS, Approved

- proposal S447 by GSI G-PAC (2017)
- [32] S. Velardita et al., Eur. Phys. J. A **59**(6), 139 (2023)
- [33] S. Bass, H. Alvarez-Pol, T. Aumann *et al.*, Prog. Part. Nucl. Phys. **41**, 255 (1998)
- [34] M. Bleicher, E. Zabrodin, C. Spieles et al., J. Phys. G: Nucl. Part. Phys. 25, 1859 (1999)
- [35] C. Rappold, T. R. Saito, O. Bertini *et al.*, Phys. Lett. B **747**, 129 (2015)
- [36] S. Navas *et al.* (Particle Data Group), Phys. Rev. D **110**, 030001 (2024)
- [37] M. S. Abdallah, B. E. Aboona, J. Adam *et al.* (STAR Collaboration), Phys. Rev. Lett. **128**, 202301 (2022)
- [38] C. Rappold, E. Kim, D. Nakajima et al., Nucl. Phys. A 913, 170 (2013)
- [39] I. Tanihata, H. Hamagaki, O. Hashimoto *et al.*, Phys. Lett. B 160, 380 (1985)
- [40] A. Boudard, J. Cugnon, J. C. David et al., Phys. Rev. C 87, 014606 (2013)
- [41] S. Leray, D. Mancusi, P. Kaitaniemi et al., J. Phys.: Conf. Ser. 420, 012065 (2013)
- [42] M. Baznat, A. Botvina, G. Musulmanbekov *et al.*, Phys. Part. Nuclei Lett. **17**, 303 (2020)
- [43] C. Bargholtz, M. Bashkanov, M. Berlowski et al., Nucl. Instrum. Methods Phys. Res. A 594, 339 (2008)
- [44] Y. K. Tanaka, P. Achenbach, H. A. Alfaki et al., Acta Phys. Pol. B Proc. Suppl. 16, 4 (2023)
- [45] R. J. M. Y. Ruber, M. Blom, H Calén et al., Nucl. Instrum. Methods Phys. Res. A 503, 431 (2003)
- [46] M. Jacewicz, PhD thesis, Uppsala University (2004)
- [47] R. Sekiya et al., Nucl. Instrum. Methods Phys. Res. A 1034, 166745 (2022)
- [48] I. Koch, Measurements of $2\pi^0$ and $3\pi^0$ Production in Proton-Proton Collisions at a Center of Mass Energy of 2.465 GeV, Ph.D. Thesis (Uppsala: Uppsala University, 2004)
- [49] E. Liu, V. Drozd, H. Ekawa et al., Nucl. Instrum. Methods Phys. Res. A 1064, 169384 (2024)
- [50] C. Rappold, E. Kim, T. R. Saito et al., Phys. Rev. C 88, 041001 (2013)
- [51] C. Rappold, T. R. Saito, O. Bertini *et al.*, Phys. Lett. B 728, 543 (2014)
- [52] H. Ekawa (WASA-FRS Collaboration), EPJ Web Conf. **271**, 08012 (2022)
- [53] T. R. Saito, P. Achenbach, H. A. Alfaki et al., Nucl. Instrum. Methods Phys. Res. B 542, 22 (2023)
- [54] S. Agostinelli, J. Allison, K. Amako et al., Nucl. Instrum. Methods Phys. Res. A 506, 250 (2003)
- [55] J. Allison, K. Amako, J. Apostolakis *et al.*, IEEE Trans. Nucl. Sci. **53**, 270 (2006)
- [56] J. Allison, K. Amako, J. Apostolakis et al., Nucl. Instrum. Methods Phys. Res. A 835, 186 (2016)
- [57] T. R. Saito, H. Ekawa, M. Nakagawa *et al.*, The Eur. Phys. J. A 57, 159 (2021)
- [58] C. Höppner, S. Neubert, B. Ketzer et al., Nucl. Instrum. Methods Phys. Res. A 620, 518 (2010)
- [59] H. Ekawa, W. Dou, Y. Gao et al., Eur. Phys. J. A 59, 103 (2023)
- [60] N. Iwasa, H. Geissel, G. Münzenberg et al., Nucl. Instrum. Methods Phys. Res. B 126, 284 (1997)
- [61] D. J. Jackson, Nucl. Instrum. Methods Phys. Res. A 388, 247 (1997)
- [62] S. Escrig, C. Rappold, J. Bernabeu *et al.*, Nucl. Instrum. Methods Phys. Res. A **1064**, 169392 (2024)